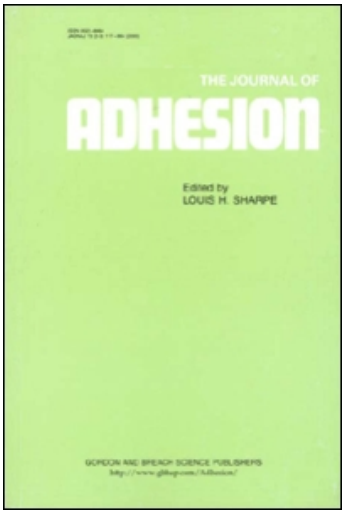

The Journal of Adhesion
Publication details, including instructions for authors and subscription information:
http://www.informaworld.com/smpp/title~content=t713453635

2-D Modeling of the Behavior of an Adhesive in an Assembly Using a Non-Associated Elasto-Visco-Plastic Model

R. Créac'hcadec[a]; J. Y. Cognard[a]
[a] Laboratoire Brestois de Mécanique et des Systèmes, ENSIETA/Université de Brest/ENIB ENSIETA, Brest, France

To cite this Article Créac'hcadec, R. and Cognard, J. Y.(2009) '2-D Modeling of the Behavior of an Adhesive in an Assembly Using a Non-Associated Elasto-Visco-Plastic Model', The Journal of Adhesion, 85: 4, 239 — 260
To link to this Article: DOI: 10.1080/00218460902881790
URL: http://dx.doi.org/10.1080/00218460902881790

The Journal of Adhesion, 85:239–260, 2009

ISSN: 0021-8464 print/1545-5823 online
DOI: 10.1080/00218460902881790

Taylor & Francis
Taylor & Francis Group

2-D Modeling of the Behavior of an Adhesive in an Assembly Using a Non-Associated Elasto-Visco-Plastic Model

R. Créac'hcadec and J. Y. Cognard
Laboratoire Brestois de Mécanique et des Systèmes, ENSIETA/ Université de Brest/ENIB ENSIETA, Brest, France

This paper presents a contribution to the development of a numerical model for an adhesive in an assembly, starting from a large data base of experimental results in the case of radial monotonic loadings. The experimental results were obtained with a modified Arcan-type fixture using specific geometries which strongly limit the influence of edge effects in order to obtain reliable information about the non-linear behavior of the adhesive. These results underline that deformations in the adhesive are much larger in shear than in peel. Thus, a non-associated 2D model, with a specific yield function, was proposed to represent accurately the experimental observations. As the stress state is not uniform in the adhesive joint for the proposed Arcan-type fixture, inverse identification techniques using non-linear finite element simulations were used. Firstly, for a given strain rate, an elasto-plastic model was proposed and its behavior was analyzed through different numerical examples. Secondly, an extension to elasto-visco-plastic models was proposed for a wide range of deformation rates under tensile-shear loading tests. Results of numerical examples and comparisons with experimental data are presented using joint-type elements (or interface elements) which allow one to limit the numerical cost in the case of bonded structures with low edge effects.

Keywords: Adhesion; Finite Element Analysis; Interface elements; Inverse technique; Modeling; Non-linear behavior

Received 14 July 2008; in final form 26 January 2009.
Presented in part at the 2nd International Conference on Advanced Computational Engineering and Experimenting (ACE-X 2008), Barcelona, Spain, 14–15 July, 2008.
Address correspondence to R. Créac'hcadec, Laboratoire Brestois de Mécanique et des Systèmes, ENSIETA/Université de Brest, 2 rue François Verny, 29806 Brest, France. E-mail: romain.creachcadec@ensieta.fr

1. INTRODUCTION

Adhesively bonded assemblies are widely used in different industries, but the prediction of the behavior of these bonded joints is still approximate due mainly to large edge effects in the adhesive joint [1]. In order to allow an optimization of industrial applications, mainly two points have to be analyzed: firstly, reliable models of the adhesive behavior have to be developed, and secondly, the use of geometries which limit the influence of edge effects can increase the transmitted load of industrial-type adhesively bonded joints. This paper presents the development of a 2D model in order to represent the non-linear behavior of an adhesive film (epoxy resin Huntsman™, Basel, Switzerland, Araldite® 420 A/B [2]) starting from a large data base of experimental results obtained by a modified Arcan fixture [3]. This fixture was designed to study the behavior of thin adhesive films up to failure in an assembly, for compression or tension to be combined with shear loads. The experimental data obtained point out viscous phenomena and dissymmetric behavior between traction and compression of the adhesive with respect to the loading conditions (tension/compression-shear). Moreover, the results underline that deformations in the adhesive are much larger in shear than in peel. It is important to notice that standard tests such as the thick adherend shear test (TAST) [4,5] or single lap shear (SLS) [6–8] specimens mostly provide information for shear loadings, not for tensile-shear loadings. Moreover, such tests are characterized with a complex stress state in the adhesive joint (especially for the SLS joint) and large edge effects which make the result analysis quite difficult [9]. In the case of the proposed Arcan–type test, specific geometries which strongly limit the influence of edge effects allow one to obtain reliable information about the non-linear behavior of the adhesive [9]. But, for a given tensile-shear loading, the stress state is not uniform in the adhesive [3]; thus, inverse identification techniques using non-linear finite element simulations have to be used in order to identify the parameters of the numerical model.

To represent the behavior of the adhesive accurately different strategies can be used, such as taking into account the influence of the hydrostatic pressure [10,11] and using non-associate elasto-visco-plastic models [12,13]. As far as 2D non-linear modeling is concerned, a specific yield function can be easily used [14,15]. Moreover, this technique is well suited to be combined with joint-type elements (or interface elements) which allow one to limit the numerical cost with respect to solid elements in the case of bonded structures with low edge effects. This type of model can be justified when the

thickness of the joint is not too large with respect to the structure dimensions [16]. The possibilities of such models have been already evaluated mainly in the case of pure shear loadings [15]. Moreover, different studies have been proposed to model strain rate effects for the adhesive [17–19].

After recalling the main points of the behavior of the studied adhesive in an assembly for a given strain rate, the development of a 2D non-associated model with specific yield function and under elasto-plastic assumption is presented in the case of radial tensile-shear loadings. The identification of the model parameters was done using a combination of an optimization software (MATLAB Mathworks Inc., Natick, MA, USA) with non-linear finite element computations realized with CAST3 M code (Saclay, CEA, France) [20]. A single lap shear-type test specimen using beaks in order to strongly limit the edge effects was analysed in order to show the response of the model under quite complex stress distribution in the adhesive. Comparisons with experimental results were also carried out. In the last part, an extension to elasto-visco-plastic models is proposed taking into account a wide range of deformation rates under tensile-shear tests.

2. PRESENTATION OF THE COMPLETE IDENTIFICATION PROCEDURE

2.1. Experimental Details

In order to study the behavior of the adhesive as a function of the normal stress component, a modified Arcan fixture was developed [3], which enables compression or tension to be combined with shear loads (Fig. 1a–b). Numerical simulations in linear elasticity, for bi-material structures, show that the use of a special geometry (Fig. 1c) for the substrate (a beak close to the adhesive joint) makes it possible to limit strongly the contribution of the singularities due to edge effects [21]. A specimen with rectangular section was proposed taking into account the problems involved in machining [3]. This experimental Arcan fixture associated with non-contact extensometry and optimization techniques allows one to analyze, for radial loadings, the non-linear behavior of an adhesive in an assembly [3]. The experimental data from Arcan tension-shear tests are defined on load-displacement diagrams (Fig. 2). *DN* and *DT* represent the relative displacements of both ends of the adhesive joint, respectively, in the normal and tangential directions of the middle plane of the adhesive [3]. They are determined at the middle of the joint length and they are considered as an approximation of the relative displacements of the entire bond

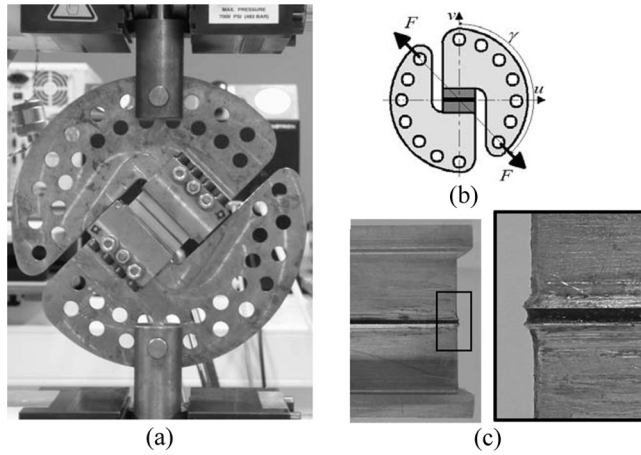

FIGURE 1 The modified Arcan fixture. (a) Presentation of a tensile-shear test, (b) principle of the Arcan Fixture, and (c) geometry of the bonded specimens.

length because the rigidities of the metallic substrates are large with respect to the adhesive one. *FN* and *FT* represent, respectively, the components of the applied load in the normal and tangential direction of the joint.

Different experimental tests have been done using epoxy resin Huntsman, Araldite 420 A/B [2], with an adhesive thickness of 0.4 mm, for monotonic radial loadings in order to characterize the non-linear mechanical behavior of the adhesive under tensile-shear loadings for a large range of strain rates. Figure 2 presents results for three loading conditions: pure shear tests (Fig. 2a, $\gamma = 90°$, Fig. 1b), pure tensile tests (Fig. 2b, $\gamma = 0°$), and tensile-shear tests (Fig. 2c–d, $\gamma = 45°$). Moreover, four crosshead displacement rates of the tensile testing machine were used to characterize the behavior of the adhesive: $V_1 = 0.01$ mm/min, $V_2 = 0.05$ mm/min, $V_3 = 0.5$ mm/min, and $V_4 = 10$ mm/min. A wide range of deformation rates is considered in order to analyze correctly the viscous effects [22]. On one hand, an important ratio, *DT*/*DN,* between the relative displacement in the normal (*DN*) and tangential (*DT*) directions is observed: this ratio can reach a range of about ten for tensile-shear tests at failure. On the other hand, an increase of the "yield stress" is observed as the strain rate increases. These viscous phenomena seem to be quite similar considering the variation of the loading direction (angle γ). Other experimental results can be found for relaxation type or cyclic loadings in [3].

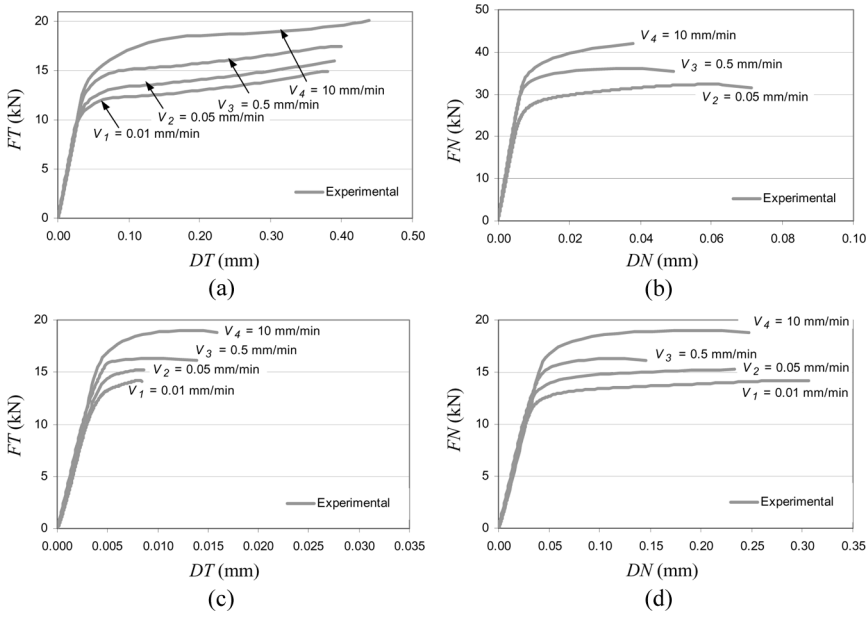

FIGURE 2 Experimental results from Arcan tension-shear tests for different radial monotonic loadings and for different displacement rates ($V_1 = 0.01\,\text{mm/min}$, $V_2 = 0.05\,\text{mm/min}$, $V_3 = 0.5\,\text{mm/min}$, and $V_4 = 10\,\text{mm/min}$). (a) Behavior in the tangential direction for pure shear tests [15] ($\gamma = 90°$, Fig. 1), (b) behavior in the normal direction for pure tensile tests ($\gamma = 0°$, Fig. 1), (c) behavior in the tangential direction for tension-shear tests ($\gamma = 45°$, Fig. 1), and (d) behavior in the normal direction for tension-shear tests ($\gamma = 45°$, Fig. 1).

2.2. Properties of Joint-Type Elements

In order to limit the numerical cost of non-linear simulations with respect to solid elements in the case of bonded structures with low edge effects, joint-type elements (or interface elements) can be used [16]. The possibilities of such elements have been already evaluated mainly in the case of pure shear loadings of adhesive joints [15]. The constitutive law for such a model is a relation between the interface tractions, $\underline{\mathbf{T}}$, and the so-called displacement jump, $[\underline{\mathbf{u}}]$, across the joint (relative displacement between $\Gamma+$ and $\Gamma-$ described in Fig. 3b). With the following relations

$$[\underline{\mathbf{u}}] = \underline{\mathbf{u}}(\Gamma+) - \underline{\mathbf{u}}(\Gamma-) = u_n \cdot \underline{\mathbf{n}} + u_s \cdot \underline{\mathbf{s}} \tag{1}$$

$$\underline{\mathbf{T}} = t_n \cdot \underline{\mathbf{n}} + t_s \cdot \underline{\mathbf{s}} \tag{2}$$

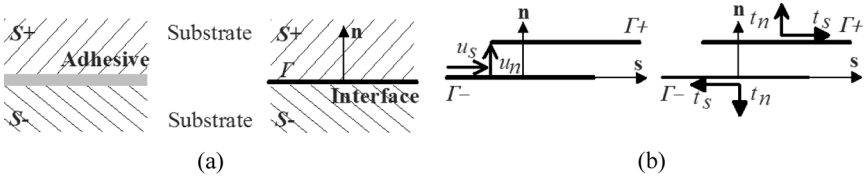

FIGURE 3 Joint model for a 2D interface [15]. (a) Geometrical modeling and (b) displacements and interface tractions.

one can define the normal and tangential relative displacements (u_n, u_s) and the normal and shear components (t_n, t_s) of the local interface traction for the interface element. Variables u_n, u_s, t_n, t_s, $\underline{\mathbf{n}}$, and $\underline{\mathbf{s}}$ are defined in Fig. 3. Using the previous notations, the elastic behavior is described as:

$$\underline{\mathbf{T}} = \begin{bmatrix} t_n \\ t_s \end{bmatrix} = \begin{bmatrix} k_n & 0 \\ 0 & k_s \end{bmatrix} \begin{bmatrix} u_n \\ u_s \end{bmatrix} = \underline{\underline{\mathbf{K_e}}}[\underline{\mathbf{u}}], \tag{3}$$

where $\underline{\underline{\mathbf{K_e}}}$ is the elastic stiffness matrix, k_n is the tensile modulus, and k_s is the shear modulus whose dimension is [F/L^3] (F and L denote force and length, respectively). It has been shown, under elastic assumption, that 2D and 3D finite element simulations with continuum elements and 2D finite element simulation with joint-type formulation give similar results [15].

2.3. Inverse Problem to be Solved

As numerical simulations performed under elasticity assumptions have pointed out that the stress distribution in the adhesive is not uniform along the adhesive joint for the modified Arcan test [3], inverse techniques have to be used. In fact, an inverse problem can be seen as a means to determine a parameter denoted by "*m,*" inaccessible by an experimental device, thanks to the measure of another parameter noted by "*d,*" directly accessible experimentally, knowing the mathematical model of the direct problem defining explicitly the value d from the value m [23]. In order to obtain the material parameters of the adhesive model starting from experimental measurements, this method often couples an analytical model [24] or a finite element model [25] to an optimization algorithm [26].

For the present problem and to determine the best values of the parameters for the model proposed in Section 3, different points have to be taken into account when solving the inverse problem due to the non-linear behavior of the adhesive. On one hand, it has been shown

that the stress distribution in the adhesive under the elastic behavior assumption depends on the elastic properties of the adhesive for a given material substrate [25]. On the other hand, the adhesive strain rate is not constant during an experimental test, contrary to the given constant displacement rate of the crosshead of the tensile machine. The experimental results give the time evolution of the relative displacements (*DT, DN*) and of the components of the load (*FT, FN*) as a function of time which are the input data for the inverse problem (Fig. 4). Figure 5 presents the time evolution of *FT, FN, DT,* and *DN* for tensile-shear ($\gamma = 45°$) tests at different displacement rates of the crosshead. Similar results are observed for pure tensile tests and pure shear tests. Thus, accurate mechanical models of the bonded specimen with quite refined space and time discretizations have to be used in order to obtain accurate numerical results.

2.4. Scheme of the Identification Problem

Figure 6 presents the 2D mechanical model used for the inverse identification procedure using the finite element code CAST3 M. It can be noted that considering adequate boundary conditions, the computation can be done on only half of the specimen. For the complete model used, the load was applied on the upper and lower straight lines of the substrates considering a uniform stress distribution and using some constraints in order to represent the high rigidity of the Arcan support. The relative displacement of the adhesive was extracted at each step of the computation at points P_1 and P_2 (Fig. 6) in the normal and tangential directions [3]. The experimental displacements were obtained close to those points with a non-contact extensometry technique [3]. Therefore, at each step of the non-linear finite element problem, the numerical values of the applied load and of the relative displacement are known. One can define the error between the experimental and numerical load-displacement curves using a quadratic function which has to be minimized. The parameters of the

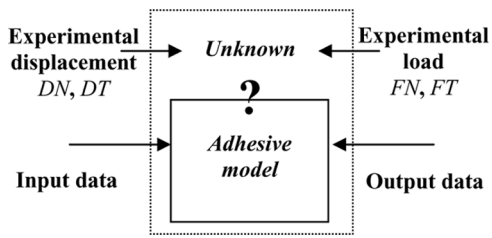

FIGURE 4 Scheme of the inverse problem for the identification of the parameters of the postulated adhesive model.

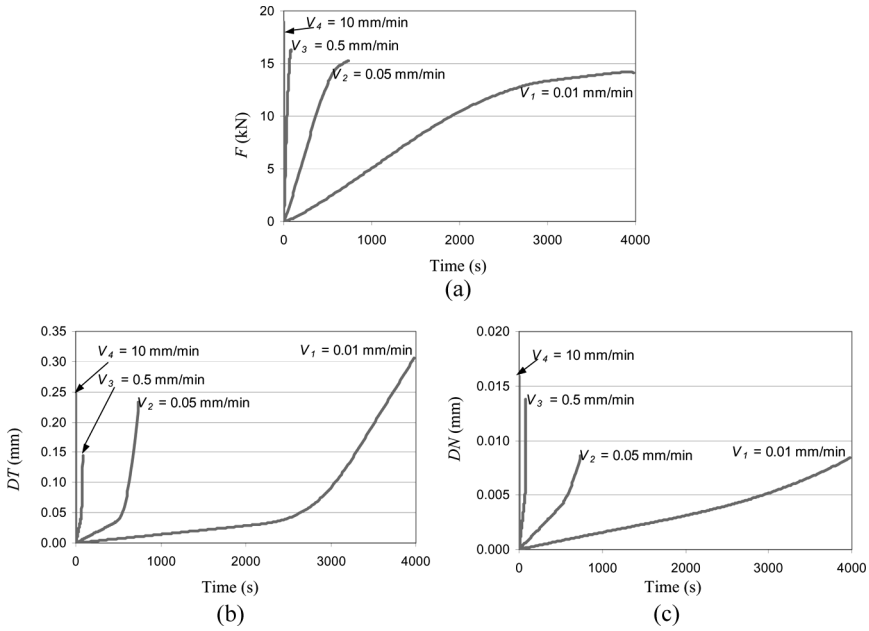

FIGURE 5 Evolution of the input data as a function of time for the inverse identification for Arcan tensile-shear tests ($\gamma = 45°$). (a) Evolution of the load (for tensile-shear tests $F = FT = FN$), (b) evolution of the tangential displacement, *DT,* and (c) evolution of the normal displacement, *DN*.

non-linear model of the adhesive have to be optimized using the experimental load-displacement curves. For the simulations, the aluminium substrates were assumed to have an elastic behavior (Young's modulus of 67 GPa and Poisson's ratio of 0.34). The finite element model was coupled to the optimization software MATLAB that generates a new set of adhesive mechanical parameters at each iteration of the optimization. The simplex algorithm used [27] gives good results.

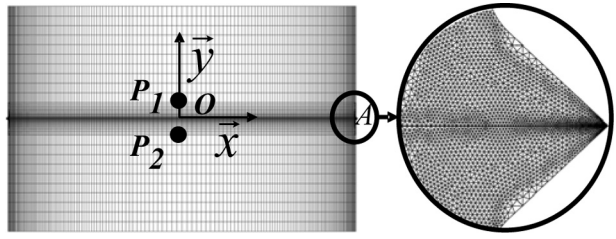

FIGURE 6 Mechanical model used for the inverse identification technique.

3. NON-ASSOCIATED ELASTO-PLASTIC MODEL

The combination of an elasto-plastic model with isotropic hardening and a specific yield function with joint-type elements allowed the accurate representation of the experimental behavior of an adhesive joint for radial loadings (especially for tensile or shear loadings) [15]. Thus, in the following, in order to take into account the differences between the deformations in the normal and tangential directions of the adhesive (Fig. 2), a non-associated approach was used [28].

3.1. Equations of the Elasto-Plastic Model

Following the framework of continuum thermodynamics [29], associated models use the normal direction to the yield surface in order to define the evolution laws and non-associated formulations introduce another function to describe the flow rules. In 2D problems, the yield surface is accurately represented with an elliptic function, f, defined from the interface tractions [14,15]. Another elliptic function, q, was used to describe the important ratio between the relative displacements in the normal and tangential directions.

The additivity of elastic $[\underline{\mathbf{u}}]^e$ and plastic $[\underline{\mathbf{u}}]^p$ (*i.e.*, irreversible) relative displacements was assumed. Thus, denoting by ρ the density and by p the plastic cumulated displacement (internal variable associated with the isotropic hardening), the free energy, $\rho\psi$, is defined as:

$$\rho\psi = \frac{1}{2} trace(\underline{\underline{\mathbf{K_e}}}[\underline{\mathbf{u}}]^{\mathrm{e}} \cdot [\underline{\mathbf{u}}]^{\mathrm{e}}) + h(p). \tag{4}$$

The state equations were obtained from the free energy:

$$\underline{\mathbf{T}} = \rho \frac{\partial \psi}{\partial [\underline{\mathbf{u}}]^{\mathrm{e}}} = \underline{\underline{\mathbf{K_e}}}[\underline{\mathbf{u}}]^{\mathrm{e}} \tag{5}$$

$$R = \rho \frac{\partial \psi}{\partial p} = h'(p) = R_i + Ap. \tag{6}$$

R is an associated variable to p and $h'(p)$ is a material function related to the isotropic hardening which can be proposed in a quite simple form for the studied adhesive and for monotonic loadings. R_i and A are characteristic parameters of the material.

The yield surface was defined with an elliptic function taking into account the differences between traction and compression (using characteristic parameters of the material: a_+, a_-, and b) [15]:

$$f = ||\underline{\mathbf{T}}|| - R = \sqrt{\frac{\langle t_n \rangle_+^2}{a_+^2} + \frac{\langle t_n \rangle_-^2}{a_-^2} + \frac{t_s^2}{b^2}} - R. \tag{7}$$

$\langle x \rangle_+$ and $\langle x \rangle_-$ are, respectively, the positive and negative part of the real x.

In order to introduce the non-associated model, an elliptic flow rule function, defined from parameters c and d, was introduced:

$$q = \sqrt{\frac{t_n^2}{c^2} + \frac{t_s^2}{d^2}} - R. \tag{8}$$

Thus, the evolution laws were defined as:

$$[\underline{\dot{\mathbf{u}}}]^{\mathrm{p}} = \dot{\lambda} \frac{\partial q}{\partial \underline{\mathbf{T}}} \tag{9}$$

$$-\dot{p} = \dot{\lambda} \frac{\partial q}{\partial R} = -\dot{\lambda}. \tag{10}$$

λ is the so-called inelastic multiplier. Therefore, in the case of an elasto-plastic behavior, for given components (t_n, t_s) of the stress vector, the direction of the inelastic displacement was defined using the normal vector at a given point of the flow rule function and was directly obtained using Eq. (9).

In order to propose an accurate model which describes the differences between tensile-shear and compression-shear loadings, it may be necessary to introduce the important ratio for the displacements at failure between the normal and tangential directions in the definition of the flow rule function as well as in the yield surface definition. But it was not introduced herein, as mainly tensile-shear loadings have been analyzed in order to validate the possibilities of the proposed non-associated model.

Moreover, the following relation is obtained [29]:

$$\lambda = \int_0^{\tau} \sqrt{([\underline{\dot{\mathbf{u}}}]^{\mathbf{p}})^{\mathrm{T}} \cdot ([\underline{\dot{\mathbf{u}}}]^{\mathbf{p}})} d\tau' = p, \tag{11}$$

where τ denotes time and subscript $^{\mathrm{T}}$ means transposition.

It is important to notice that the different parameters are not independent and, thus, parameters b and d can be chosen equal to 1. Therefore, this non-associated elasto-plastic model is defined using seven parameters (Table 1).

The implementation of this model in the finite element code CAST3 M was realized using a return mapping-type algorithm [30]. A presentation of such a numerical integration approach can be found in [15] in the case of the associated model.

TABLE 1 Material Parameters of the Adhesive Non-Associated Elasto-Plastic Model

Parameters	Values
k_n (N/mm^3)	5575
k_s (N/mm^3)	1015
a_+	2.05
a_-	4
c	3.3
R_i(MPa)	22
A (N/mm^3)	14

3.2. Results for Tensile-Shear Radial Monotonic Loadings

The inverse identification technique was realized using, simultaneously, all the experimental database as the model must represent the behavior of the adhesive for the different monotonic radial loadings. Experimental results for $\gamma = 0°$, $30°$, $37.5°$, $45°$, and $90°$, obtained for a displacement rate of 0.5 mm/min, were used (various effects are observed between $0°$ and $45°$). Table 1 gives the values of material parameters of the non-associated elasto-plastic model, obtained with the inverse identification method.

Figure 7 presents, for the different radial loadings, comparisons between experimental data and results of finite element simulations using the adhesive parameters defined in Table 1. Figure 7a shows the yield surface and the so-called flow function which were obtained. The experimental results (denoted by "Experimental") and the numerical results obtained by the finite element simulations (denoted by "FEA") are plotted on the same load-displacement graph in Figs. 7b and 7c. The results of the proposed model are in good agreement with the experimental data. The chosen flow rule function allows the accurate representation of the large ratio between the inelastic displacements in the normal and tangential directions.

Figure 8 shows the results for the tensile-shear test at $\gamma = 45°$, which is the most difficult test to represent. Figures 8a and 8b present the experimental and numerical load-displacement curves. Figures 8c and 8d represent the evolution of the adhesive shear and peel stresses along half of the overlap (segment [OA] defined in Fig. 6) for increasing stages of loading (the different steps: i, j, k, and l are defined on Figs. 8a and 8b). After the known non-uniform stress distribution in the elastic domain (i), the stresses became nearly uniform for large inelastic displacements (before failure) (l). In the transition part (j–k), large stress re-distributions are observed associated with the

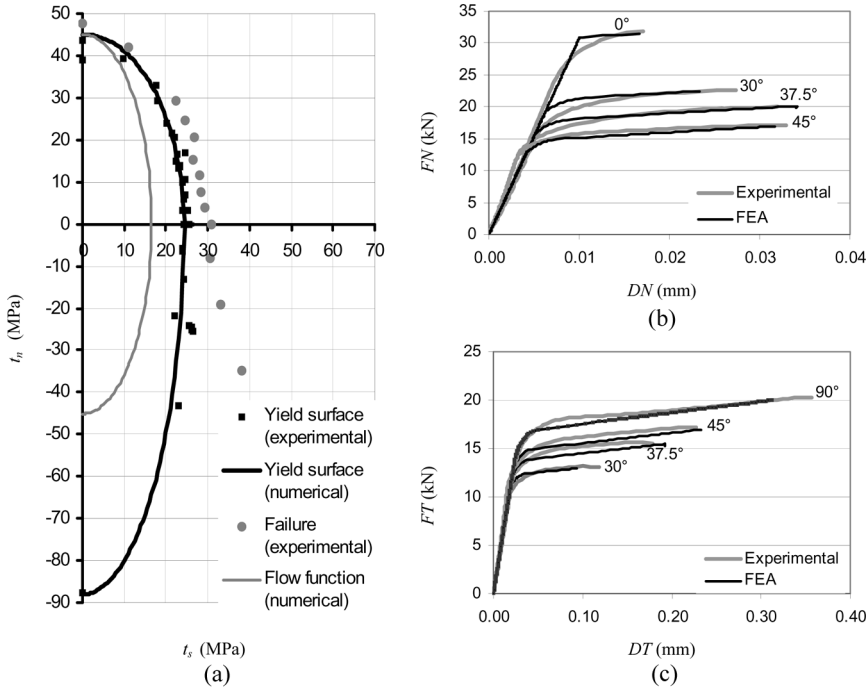

FIGURE 7 Comparison between experimental ("Experimental" in graphs) and finite element analysis ("FEA" in graphs) Arcan results for different radial loadings ($\gamma = 0°$, 30°, 37.5°, 45°, 90°). (a) Identified yield surface and flow law, (b) adhesive behavior in the normal direction, and (c) adhesive behavior in the tangential direction.

development of plasticity in the adhesive. Nearly the same evolution of the stress distribution in the adhesive was observed for the different radial loadings.

3.3. Validation Example: A Simple Lap Shear Specimen with Beaks

In order to validate the possibilities of the proposed model in the case of bonded structures with low edge effects, an example with more complex stress distribution is presented. A simple lap shear-type specimen with thick substrates and beaks was designed to analyze the influence of different parameters [31]. The substrates were machined with the greatest care and a precise positioning of the substrates was obtained. Moreover, the thickness of the bondline was controlled during the

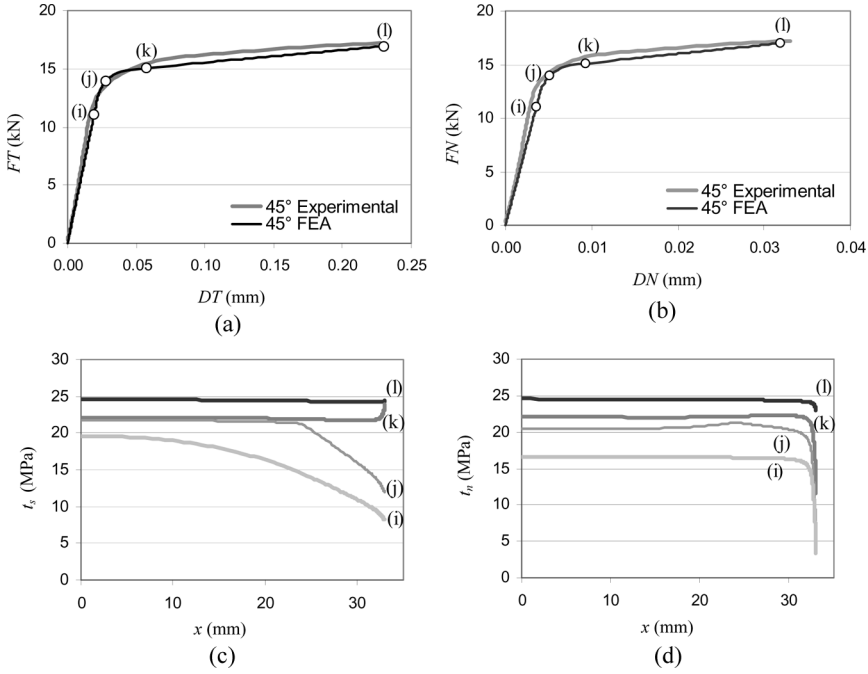

FIGURE 8 Comparison between experimental ("Experimental" in graphs) and finite element analysis ("FEA" in graphs) Arcan results for tensile-shear loading ($\gamma = 45°$) at a displacement rate of 0.5 mm/min. (a) Load-displacement diagram in the tangential direction, (b) load-displacement diagram in the normal direction, (c) evolution of the shear stress distribution in the adhesive for different steps (i, j, k, l) along half of the overlap, and (d) evolution of the normal stress distribution in the adhesive for different steps (i, j, k, l) along half of the overlap.

bonding process (Fig. 9a). Measurements were taken in order to verify the behavior of the specimen during the fixing and loading phases (Fig. 9c). The main dimensions of the bonded specimen are: $d_1 = 66$ mm, $d_2 = 325$ mm, $d_3 = 56$ mm, $d_4 = 20$ mm, $d_5 = 40$ mm, and $d_6 = 20$ mm (Figs. 9d and 9e). The complete analysis of this experimental test requires comparison between experimental and numerical results. The finite element model takes into account the beaks, and the adhesive was meshed with nearly 400 six-node interface elements. The computation can be made in 2D using half of the model by applying adequate boundary conditions. The prescribed displacements followed a linear time evolution. The maximum value of the displacement was $Ud = 0.7$ mm (Fig. 9d).

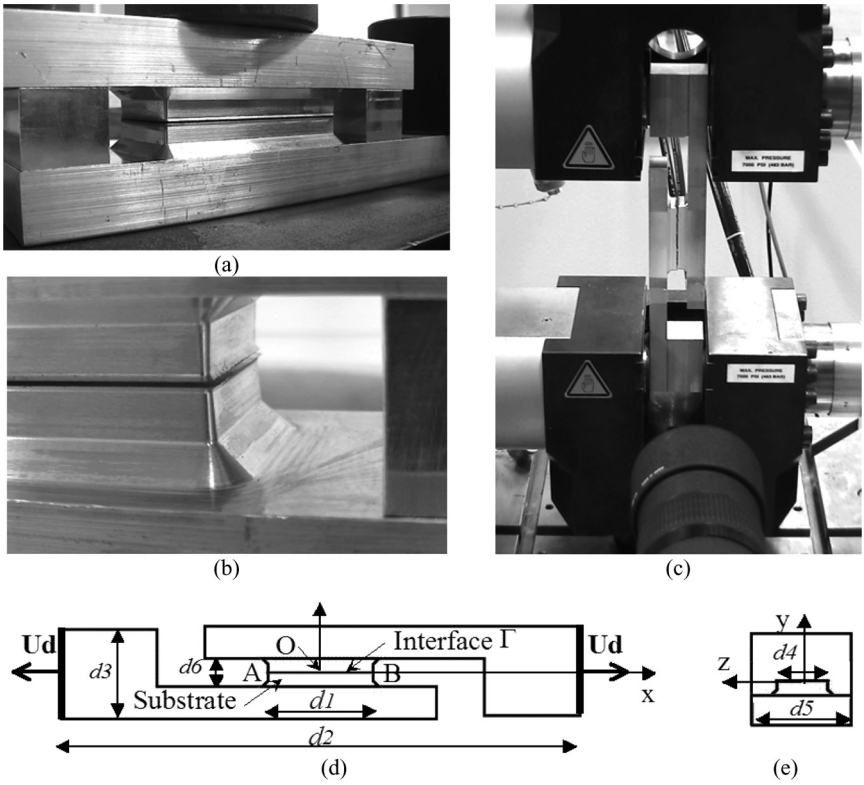

FIGURE 9 Simple lap shear type specimen with thick substrates and beaks. (a) Manufacturing of the specimen, (b) geometry of the substrates, (c) experimental test, (d) 2D numerical model, and (e) geometry in the z-direction.

Figure 10f shows the comparison between the experimental and numerical results in the load-displacement curves and underlines the accuracy of the response of the proposed model for this quite complex specimen. Figure 10 presents the evolution of the components of the stresses, the components of the relative displacements, and the plastic cumulated displacement in the adhesive with respect to the segment [*OB*] (Fig. 9d) for different values of the prescribed displacement presented in Figure 10f. The non-linear behavior first appears close to the two ends of the bonded joint. Large stress redistribution can be noted in the adhesive, especially for the normal stress. For a complete plastified adhesive, a more constant stress distribution in the adhesive is obtained. For this kind of joint, the peak values reached by the normal stresses are on the same level as the tangential

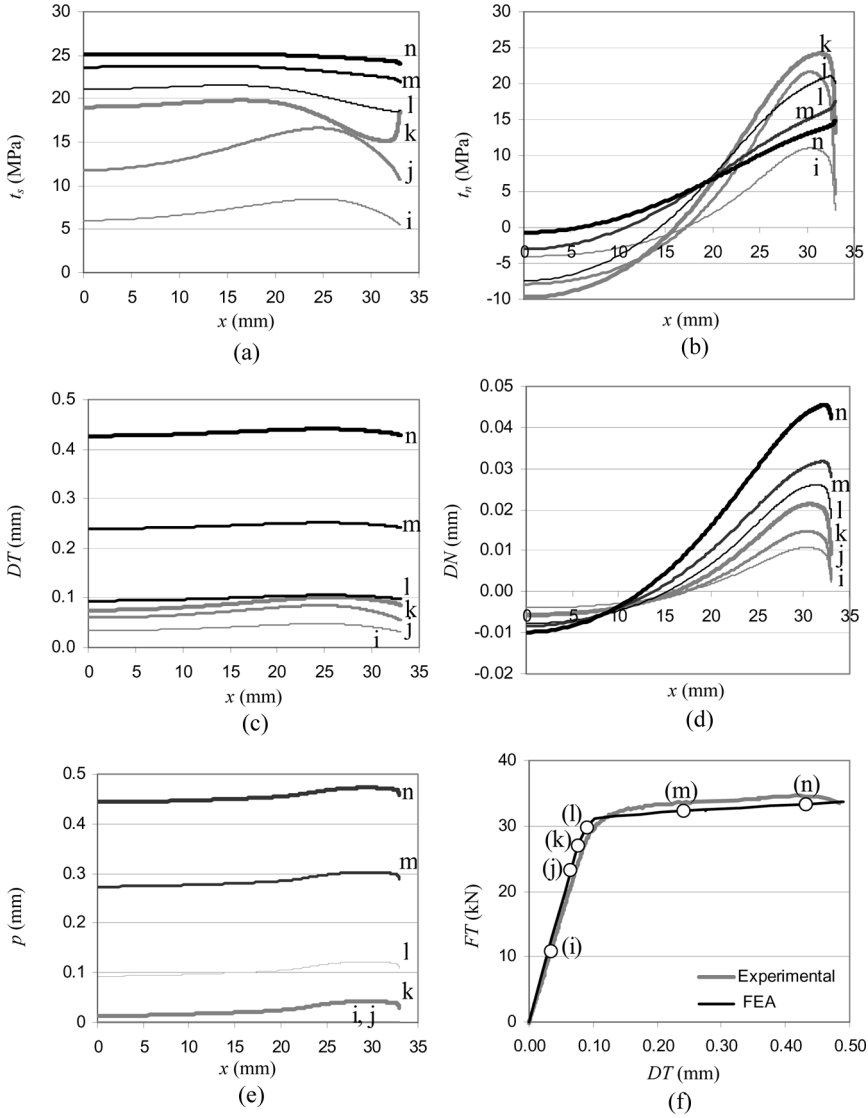

FIGURE 10 Simple lap shear specimen with beaks and thick substrates: evolution of different parameters along half of the adhesive joint (steps i, j, k, l, m, and n). (a) Shear stress t_s, (b) normal stress t_n, (c) tangential displacement, DT, (d) normal displacement, DN, (e) cumulated plastic displacement, p, and (f) load-displacement diagram for experimental and numerical results.

ones. Figures 10c and 10d underline the differences in terms of relative displacements between the normal and tangential directions (a ratio of nearly ten is obtained). One can notice that for such simple lap shear specimens, the stress distribution in the adhesive is quite complex, even with thick substrates. Thus, for the analysis of such tests, the influence of the peel stress and the normal displacement component cannot be neglected.

These results illustrate the possibilities of the proposed strategy for modeling the behavior of adhesive bonded assemblies associated with low edges effects. In order to complete the numerical analysis, a failure criterion has to be defined. Moreover, for such non-associated models, one must analyze the stability conditions of the integration law behavior scheme [32].

4. NON-ASSOCIATED ELASTO-VISCO-PLASTIC MODEL

4.1. Equations of the Elasto-Visco-Plastic Model

For the sake of simplicity, the same notations as those used for the elasto-plastic model were used in order to describe the equations of the non-associated elasto-visco-plastic model. The state Eqs. (5) and (6), the yield surface (7), and the flow rule function (8) defined for the elasto-plastic model were conserved [29]. Only the new evolution laws have to be defined. The rate effects were described using the Nouailhas type potential, Ω [15, 33]:

$$\Omega = \frac{K}{\alpha(n+1)} \exp\left(\alpha \left\langle \frac{q}{K} \right\rangle^{n+1}\right), \tag{12}$$

where K, α, and n are characteristic parameters of the material and q is defined by Eq. (8). Thus, one obtains the evolution law for the inelastic displacement:

$$[\dot{\underline{\mathbf{u}}}]^p = \frac{\partial \Omega}{\partial \underline{\mathbf{T}}} = \frac{\partial \Omega}{\partial q} \cdot \frac{\partial q}{\partial \underline{\mathbf{T}}}. \tag{13}$$

4.2. Numerical Integration of the Constitutive Equations

For the numerical integration of the elasto-visco-plastic constitutive equations, the strategy proposed by Corigliano and Ricci was followed [34]. The integration scheme is based on a Runge-Kutta type algorithm. On a time step $t \in [t_n,\ t_{n+1}]$ knowing the variables for t_n ($[\underline{\mathbf{u}}]_n$, $\underline{\mathbf{T}}_n$,λ_n) and for a given $\Delta[\underline{\mathbf{u}}]$ ($\Delta[\underline{\mathbf{u}}] = [\underline{\mathbf{u}}]_{n+1} - [\underline{\mathbf{u}}]_n$), the problem is to integrate the constitutive relations in order to determine the different

variables at time t_{n+1} (i.e., $\underline{\mathbf{T}}_{n+1}$ and λ_{n+1} or $\Delta\underline{\mathbf{T}} = \underline{\mathbf{T}}_{n+1} - \underline{\mathbf{T}}_n$ and $\Delta\lambda = \lambda_{n+1} - \lambda_n$). A mid-point approximation governed by parameter $\theta \in [0,1]$ was introduced for the unknown inelastic displacement $[\underline{\dot{\mathbf{u}}}]^p_{n+1}$ and for the inelastic multiplier λ_{n+1} . The corresponding rate quantities $[\underline{\mathbf{u}}]^p_{n+1}$ and $\dot{\lambda}_{n+1}$ were expanded in a Taylor series up to the first order.

If $f \leq 0$ (elastic behavior over the time step)

$$\begin{cases} \underline{\mathbf{T}}_{n+1} = \underline{\underline{\mathbf{K}}}_{\mathbf{e}}([\underline{\mathbf{u}}]_{n+1} - [\underline{\mathbf{u}}]^p_n) \\ [\underline{\mathbf{u}}]^p_{n+1} = [\underline{\mathbf{u}}]^p_n \\ \lambda_{n+1} = \lambda_n. \end{cases} \tag{14}$$

If $f > 0$ (elasto-visco-plastic behavior over the time step)

$$\begin{cases} \underline{\mathbf{T}}_{n+1} = \underline{\underline{\mathbf{K}}}_{\mathbf{e}}([\underline{\mathbf{u}}]_{n+1} - [\underline{\mathbf{u}}]^p_n) \\ [\underline{\mathbf{u}}]^p_{n+1} = [\underline{\mathbf{u}}]^p_n + \Delta\tau((1-\theta)[\underline{\dot{\mathbf{u}}}]^p_n + \theta[\underline{\dot{\mathbf{u}}}]^p_{n+1}) \\ \lambda_{n+1} = \lambda_n + \Delta\tau((1-\theta)\dot{\lambda}_n + \theta\dot{\lambda}_{n+1}) \\ [\underline{\dot{\mathbf{u}}}]^p_{n+1} = [\underline{\dot{\mathbf{u}}}]^p_n + \left(\dfrac{\partial[\underline{\dot{\mathbf{u}}}]^p}{\partial\underline{\mathbf{T}}}|_n\right)^{\mathbf{T}} \Delta\underline{\mathbf{T}} + \left(\dfrac{\partial[\underline{\dot{\mathbf{u}}}]^p}{\partial\lambda}|_n\right)^{\mathbf{T}} \Delta\lambda \\ \dot{\lambda}_{n+1} = \dot{\lambda}_n + \left(\dfrac{\partial\dot{\lambda}}{\partial[\underline{\dot{\mathbf{u}}}]^p}\bigg|_n\right)^{\mathbf{T}} \Delta[\underline{\dot{\mathbf{u}}}]^p. \end{cases} \tag{15}$$

$\underline{\mathbf{T}}_{n+1}$ can be then explicitly written using Eq. (15). The details of the calculations can be found in [34]. The parameter θ was choosen equal to 0.5 according to the stability of the integration method proposed by Corrigliano and Ricci and numerical responses were computed with a time step of $\Delta\tau = 0.001$ s to avoid numerical instability.

4.3. Results for Tensile-Shear Radial Monotonic Loadings

The inverse identification technique was done using, simultaneously, the experimental results for three monotonic radial loadings ($\gamma = 0^\circ$, 45°, and 90°) and for four displacement rates of the crosshead of the tensile testing machine ($V_1 = 0.01$ mm/min, $V_2 = 0.05$ mm/min, $V_3 = 0.5$ mm/min, and $V_4 = 10$ mm/min). Table 2 gives the obtained values of material parameters of the non-associated elasto-visco-plastic model.

Figure 11 presents comparisons between experimental data (denoted by "Experimental") and results of finite element simulations (denoted by "FEA") using the adhesive parameters obtained with the inverse identification. The load-displacement curves obtained with

TABLE 2 Material Parameters of the Adhesive Non-Associated Elasto-Visco-Plastic Model

Parameters	Values
k_n (N/mm^3)	5575
k_s (N/mm^3)	1015
a_+	2.3
a_-	4
c	3.8
R_i (MPa)	20
A (N/mm^3)	13
n	1
K	2050
α	1

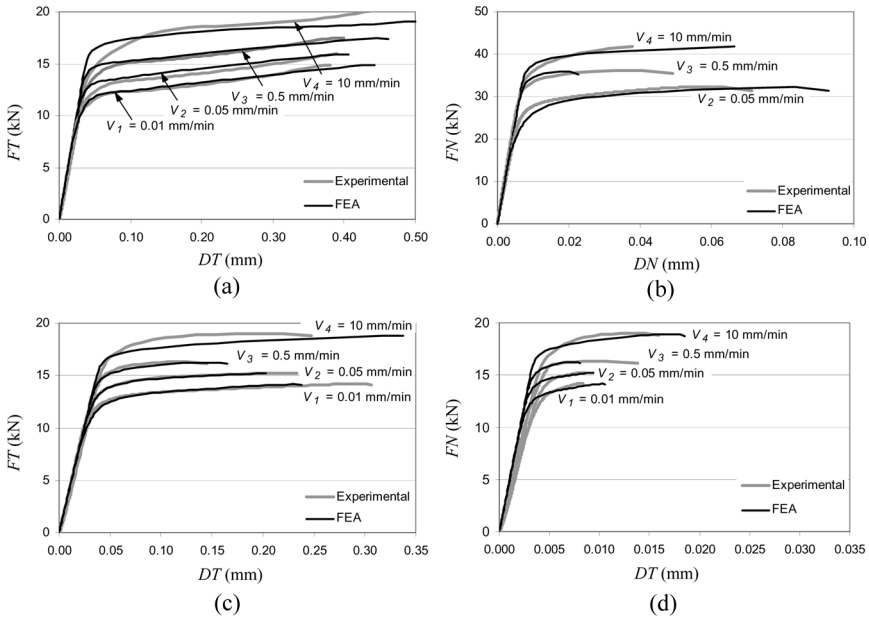

FIGURE 11 Comparison between experimental ("Experimental" in graphs) and finite element analysis ("FEA" in graphs) load-displacement Arcan curves for different radial monotonic loadings and for different displacement rates ($V_1 = 0.01$ mm/min, $V_2 = 0.05$ mm/min, $V_3 = 0.5$ mm/min, and $V_4 = 10$ mm/min). (a) Behavior in the tangential direction for pure shear tests [15], (b) behavior in the normal direction for pure tensile tests, (c) behavior in the tangential direction for tensile-shear tests ($\gamma = 45°$), and (d) behavior in the normal direction for tension-shear tests ($\gamma = 45°$).

the proposed model are in good agreement with the experimental ones, taking into account the large ratio between the inelastic displacements in the normal and tangential directions, for a large range of radial monotonic loadings.

Figure 12 presents the results for the tensile-shear test at $\gamma = 45°$ and for a displacement rate of the crosshead of $V_1 = 0.01\,\text{mm/min}$. Comparisons are shown in terms of load-displacement curves between experimental and numerical results. Moreover, the evolutions of the shear and peel stresses along half of the adhesive (segment [OA], Fig. 6) are presented for increasing stages of loading. The results presented in Fig. 8 for a displacement rate of $V_3 = 0.5\,\text{mm/min}$ and on Fig. 12 for a displacement rate of $V_1 = 0.01\,\text{mm/min}$ underline the influence of the loading rate on the stress distribution in the adhesive.

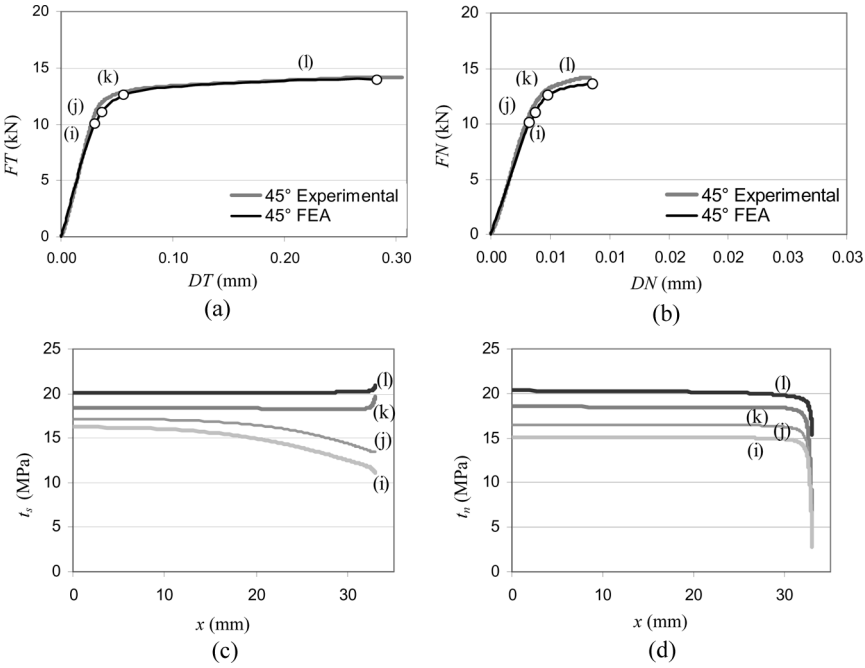

FIGURE 12 Comparison between experimental ("Experimental" in graphs) and finite element analysis ("FEA" in graphs) Arcan results for tensile-shear loading ($\gamma = 45°$) at a displacement rate of 0.01 mm/min. (a) Load-displacement diagram in the tangential direction, (b) load-displacement diagram in the normal direction, (c) shear stress distribution in the middle of the adhesive for different steps (i, j, k, and l) along half of the overlap (x), and (d) normal stress distribution in the middle of the adhesive for different steps (i, j, k, and l) along half of the overlap (x).

4.4. Validation Example: A Simple Lap Shear Specimen with Beaks

The simple lap shear type specimen with thick substrates and beaks presented in Fig. 9 was used to analyze numerically the influence of the loading rate on the stress distribution in the adhesive. Figures 13b–d present, for different time steps (i, j, and k) defined in Fig. 13a, the stress distribution in the normal and tangential directions along half of the overlap [OB] (Fig. 9d). Results show the influence of the loading rate stress distribution in the adhesive and, therefore, on the global response of the structure. Figure 13 also shows the possibilities of the proposed strategy for modeling the behavior of adhesive bonded assemblies associated with low edges effects.

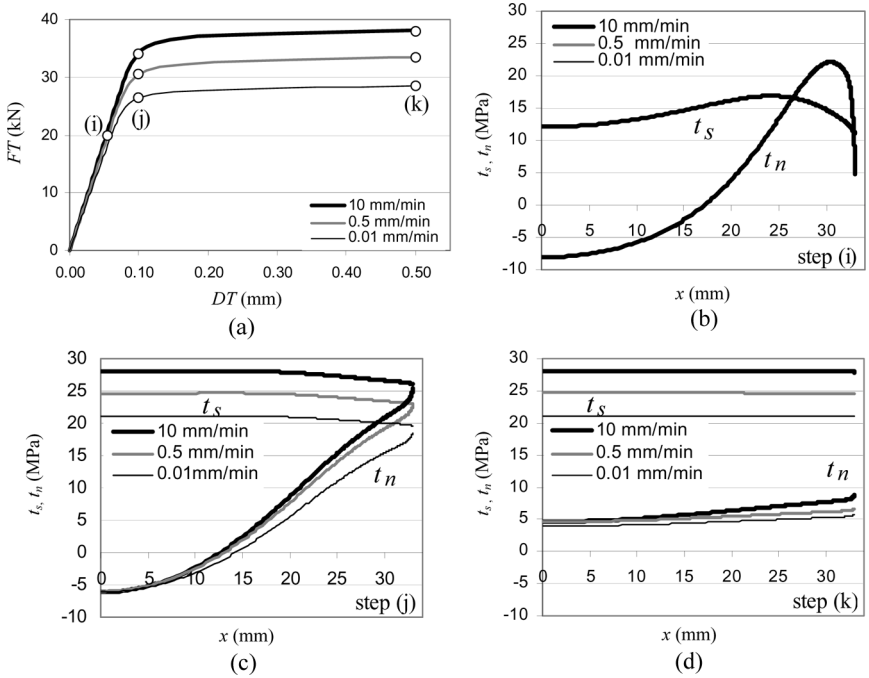

FIGURE 13 Finite element analysis for a simple lap shear specimen with beaks at three displacement rates $V_1 = 0.01\,\text{mm/min}$, $V_3 = 0.5\,\text{mm/min}$, $V_4 = 10\,\text{mm/min}$ for different steps of displacement (i, j, and k). (a) Load-displacement curves in the tangential direction, (b, c, and d) evolution of the shear, t_s, and the tensile, t_n, stresses for different steps (i, j, and k) along half of the overlap.

5. CONCLUSIONS

The optimization of adhesively bonded assemblies, which are widely used in different industries, requires accurate numerical models. However, the experimental and numerical analyses of the mechanical behavior of bonded joints can be particularly difficult due to the edge effects. This paper presents a contribution to the development of an accurate numerical model for an adhesive in an assembly, starting from a large database of experimental results in the case of radial monotonic loadings. The experimental results were obtained with a modified Arcan-type fixture using specific geometries which strongly limit the influence of edge effects. A non-associated 2D model was proposed to represent accurately the experimental observations and, in particular, the much larger deformation in shear than in peel. The responses (load-displacement curves) of the proposed model, using few material parameters, are in good agreement with the experimental data in the case of a wide range of deformation rates under different tensile-shear loading tests.

The numerical implementation of the proposed model was done using joint-type elements (or interface elements) which allow the limitation of the numerical cost in the case of bonded structures with low edge effects. Comparisons between numerical and experimental results, in the case of a bonded specimen characterized with a quite complex stress distribution, illustrate the possibilities of the proposed strategy for modeling the behavior of adhesive bonded assemblies.

This work will be further developed in order to analyze the stability conditions for such non-associated models and to study more efficient numerical integration techniques in order reduce the numerical costs. Moreover, the model needs to be extended to describe accurately the adhesive behavior under cyclic- and relaxation-type loadings. It is also important to notice that the proposed model can be adapted to solid finite elements, using finite strain formulations, for analyzing the response of industrial-type structures with edge effects.

ACKNOWLEDGMENTS

The authors are grateful to Laurent Sohier from Laboratoire Brestois de Mécanique et des Systèmes, Université de Brest for his contribution in the experimental results used in this paper.

REFERENCES

[1] Adams, R. D., (Woodhead Publishing Ltd., University of Bristol, UK, 2005).
[2] Huntsman™ Structural Adhesives – Araldite® 420 A/B, Publication No. A 161, Duxford, UK, (2004).

[3] Cognard, J. Y., Davies, P., Sohier, L., and Créac'hcadec, R., *Composite Structures* **76**, 34–46 (2006).
[4] ASTM D5656-95, Standard Test Method for Thick-Adherend Metal Lap-Shear Joints for Determination of the Stress-Strain Behavior of Adhesives in Shear by Tension Loading, (American Society of Testing and Materials, West Conshohocken, PA, 1995).
[5] Maheri, M. R. and Adams, R. D., *Int. J. Adhesion Adhesives* **22**, 119–127 (2002).
[6] ISO 15108, 1998, Adhesives—Determination of strength of bonded joints using a bending-shear method, (ISO Copyright Office, Geneva, Switzerland, 1998).
[7] Zgoul, M. and Crocombe, A. D., *Int. J. Adhesion Adhesives*, **24**, 355–366 (2004).
[8] Lee, J. and Kim, H., *J. Adhesion* **83**, 837–870 (2007).
[9] Cognard, J. Y., Créac'hcadec, R., Sohier, L., and Davies, P., *Int. J. Adhesion Adhesives.* **28**, 393–404 (2008).
[10] Deb, A., Malvade, I., Biswas, P., and Schroeder, J., *Int. J. Adhesion Adhesives.* **28**, 1–15 (2008).
[11] Dean, G. D., Read, B. E., and Duncan, B. C., Project PAJ2—An evaluation of yield criteria for adhesives for finite element analysis. Report No. 7, (NPL Report, Boston Spa, UK, 1998). CMMT(A), 117.
[12] Rolfres, R., Volger, M., Ernst, G., and Hühne, C., *Trends in Computational Structures Technology*, (Saxe-Coburg Publications, Stirling, UK, 2008). Chap. 7, pp 151–171.
[13] Mahnken, R. and Schlimmer, M., *Int. J. Numer. Meth. Engng.* **63**, 1461–1477 (2005).
[14] Keller, T. and Vallée, T., *Composites Part B: Engineering* **36**, 341–350 (2005).
[15] Créac'hcadec, R., Cognard, J. Y., and Heuzé, T., *J. Adhesion Sci. and Technol.* **22**, 1541–1563 (2008).
[16] Allix, O. and Corigliano, A., *Int. J. Solids Structures* **36**, 2189–2216 (1999).
[17] Chiu, J. W. K., Chalkley, P. D., and Jones, R., *Computers & Structures* **53**, 483–489 (1994).
[18] Chiu, J. W. K. and Jones, R., *Int. J. Adhesion Adhesives* **15**, 131–136 (1995).
[19] Zgoul, M. and Crocombe, A. D., *Int. J. Adhesion Adhesives* **24**, 355–366 (2004).
[20] Cognard, J. Y., Thomas, F., and Verpeaux, P., *Advances in Engineering Software* **31**, 885–899 (2000).
[21] Cognard, J. Y., *Computer & Structures* **86**, 1704–1717 (2008).
[22] Rémond, Y., *Composites Sci. and Technol.* **65**, 421–428 (2005).
[23] Arnst, M., Clouteau, D., and Bonnet, M., *Computer Methods in Applied Mechanics and Engineering* **197**, 589–608 (2008).
[24] Alfredsson, K. S., *Int. J. Fracture* **123**, 49–62 (2003).
[25] Öchsner, A. and Gegner, J., *Int. J. Adhesion Adhesives* **21**, 349–353 (2001).
[26] Kang, Y. L., Lin, X. H., and Qin, Q. H., *Composite Structures* **66**, 449–458 (2004).
[27] Bixby, R. E., *ORSA J. Computing* **4**, 267–284 (1992).
[28] Stoughton, T. B. and Yoon, J. W., *Int. J. Plasticity* **20**, 705–731 (2000).
[29] Lemaitre, J. and Chaboche, J. L., *Mechanics of Solid Materials*, (Cambridge University Press, 1994).
[30] Simo, J. C. and Taylor, R. L., *Int. J. for Numerical Methods in Engineering* **22**, 649 (1986).
[31] Cognard, J. Y., Créac'hcadec, R., Davies, P., and Sohier, L., *Innovation in Engineering Computational Structures*, (Saxe-Coburg Publications, Stirling, UK, 2006). Chap. 11, pp 225–247.
[32] Famiyesin, O. O. R., *Computers & Structures* **79**, 1233–1250 (2001).
[33] Nouaihlas, D., *Int. J. Plasticity* **5**, 501–520 (1989).
[34] Corigliano, A. and Ricci, M., *Int. J. Solids Structures* **38**, 547–576 (2001).